Check for updates

ADVANCED ENGINEERING MATERIALS
www.aem-journal.com

Automated Workflow for Phase-Field Simulations: Unveiling the Impact of Heat-Treatment Parameters on Bainitic Microstructure in Steel

Dhanunjaya K. Nerella, Muhammad Adil Ali, Hesham Salama, Oguz Gulbay, Marc Ackermann, Oleg Shchyglo, Ulrich Krupp, and Ingo Steinbach*

Bainitic steels are extensively utilized across various sectors, such as the automotive and railway industries, owing to their impressive mechanical properties, including strength, hardness, and fatigue resistance. However, the pursuit of achieving the desired optimal mechanical properties presents considerable challenges due to the intricate bainitic microstructures consisting of multiple phases. To tackle these challenges, an automated workflow is used for extracting 2D and 3D microstructural features. The proposed method allows for a detailed examination of the correlations between microstructure characteristics and the processing parameters, specifically the holding temperature during transformation. In these findings, it is revealed that as the holding temperature decreases, there is a notable reduction in microstructural element size and carbon partitioning. Some of the observations are microstructural features such as area, perimeter, and thickness of the bainitic ferrite grains under two different holding temperatures. Phase-field simulations results show that the microstructures at lower holding temperatures have finer grains. The distributions of grain areas and perimeters are uniform, with smaller grains dominating at low and high isothermal holding temperatures. While the grain thickness measurements from simulations and experiments at high temperature are qualitatively aligned, data from low temperatures show discrepancies.

1. Introduction

Bainitic steels have many engineering applications due to their good mechanical properties. Because of their enhanced fatigue and wear resistance properties, they are widely used in the railway industry and in automotive applications such as gears and bearings.[1] Bainitic microstructures, which are responsible for obtaining good mechanical properties, are dependent on chemical composition and processing parameters, e.g., heat treatment. Thus, there is a strong relationship between the process–structure–property for bainitic steels. In the context of bainitic microstructures, it still remains controversial whether it is formed in a diffusion-controlled or deformation-controlled manner.[2] Bainitic microstructures are complex in nature consisting of a wide range of morphologies like laths of bainitic ferrite (BF), martensite–austenite (MA) islands observed in low-carbon alloys with Si, Mn, and Cr, retained austenite (RA) films and carbide precipitates observed in Fe—C alloys with Mn and Cr.[3] Identification and segmentation of MA islands using deep-learning methods were implemented in ref. [4], where the morphological features of the MA islands are studied. Widths of BF and RA were studied in refs. [3,5], BF plate misorientation analysis was carried out in ref. [6]. Length of the BF laths was studied in ref. [7].

Since most of the experimental studies are carried out in 2D, the microstructure analysis is typically limited to 2D. Morphological analysis of BF is limited in existing studies where the morphological feature extraction of BF is limited to not more than two. Complete feature extraction of BF is complex because of its morphology and 3D morphological feature extraction of BF is extremely difficult to perform experimentally. In contrast, phase-field (PF) simulations can deliver realistic microstructures comparable to experimental results.[8] Subsequently the 3D microstructural features from PF simulations can be used to study the process–structure–property relationships. Analysis of microstructures from the PF method using n-point statistics was described in refs. [9,10].

Computational materials science in general and theoretical PF simulations in particular are witnessing a remarkable surge in

D. K. Nerella, M. A. Ali, H. Salama, O. Shchyglo, I. Steinbach
Interdisciplinary Centre for Advanced Materials Simulation
Ruhr-Universität Bochum
Universität Str. 150, 44801 Bochum, Germany
E-mail: dhanunjaya.nerella@rub.de

O. Gulbay, M. Ackermann, U. Krupp
Steel Institute
RWTH Aachen University
52072 Aachen, Germany

The ORCID identification number(s) for the author(s) of this article can be found under https://doi.org/10.1002/adem.202400905.

© 2024 The Author(s). Advanced Engineering Materials published by Wiley-VCH GmbH. This is an open access article under the terms of the Creative Commons Attribution-NonCommercial-NoDerivs License, which permits use and distribution in any medium, provided the original work is properly cited, the use is non-commercial and no modifications or adaptations are made.

DOI: 10.1002/adem.202400905

predictive capabilities owing to continual advancements in theoretical frameworks, computing technologies, and software development. As researchers aim to construct comprehensive databases of materials properties, they encounter the formidable task of executing numerous computations, potentially reaching into the thousands. The complexities involved in generating input files and troubleshooting errors encountered during these computational efforts pose increasingly challenging obstacles. Moreover, the absence of well-documented procedures complicates the process of mastering diverse analysis techniques, leading to inefficiencies in tool utilization. Often, certain calculations entail labor-intensive steps vulnerable to human errors. To overcome these challenges, implementing automated workflows emerges as a crucial strategy with numerous advantages. By simplifying the execution of calculations, these workflows free researchers from the tedious details of computational tasks, enabling them to focus on the core scientific aspects of their work. Furthermore, by introducing standardized protocols for simulations, these workflows promote reproducibility and facilitate thorough testing of hypotheses. Additionally, they empower researchers to undertake extensive explorations of high-dimensional materials parameter spaces, a task that would otherwise be excessively time-consuming.[11,12]

Successful implementations of automated workflows are both diverse and promising. For instance, Nikolaev et al.[13] have made significant strides in realizing automated rapid serial experimentation, marking a substantial leap toward autonomous closed-loop learning systems. Similarly, Dimitrov et al.[14] have developed an autonomous system for molecular synthesis and characterization. Additionally, Matthew et al.[12] have elucidated a comprehensive framework for conducting atomistic simulations of materials, underscoring the versatility of automated workflows across different domains. There are readily available commercial[15] and open-source workflow managers[16] for theoretical simulations and data analysis which greatly simplify computational science efforts in industry and academia.

In the present study, we introduce an automated workflow tailored to establish a nuanced relationship between heat-treatment parameters and microstructural features, leveraging PF simulation results. Through the seamless integration of computational methodologies, our approach promises to unravel intricate correlations between heat-treatment parameters and microstructural features (**Figure 1**).

2. Theoretical Background and Methodology

2.1. Workflow Implementation

The workflow in this study integrates a variety of computational tools and libraries, all coordinated through the Python programming language.[17] The approach begins with the generation of microstructures, simulated by the OpenPhase software tool[18–20] which is a software library implementing the PF method. It offers a robust platform for simulating microstructural evolution under predefined conditions. It requires an input file that defines various parameters such as alloy composition, mechanical properties, heat-treatment conditions, and numerical discretization parameters. Upon successful completion of the simulation, OpenPhase outputs the data in a *.vtk* file format which is then converted to *.csv* to streamline post-processing analysis. Subsequently, Python libraries such as PIL[21] and OpenCV,[22] widely recognized for their ability in image analysis, are employed for 2D microstructure analysis. The typical microstructural features which can be extracted from the simulations are listed in **Table 1**. A single BF variant with a unique index (from simulation) is considered as a "grain" for morphological feature analysis. Furthermore, 3D information, including the volume of grains, is subsequently calculated.

2.2. Bainitic Microstructure

To simulate the bainite microstructure, 3D simulations were carried out for a binary Fe—C steel with 0.2 wt% carbon. The simulations were performed in a simulation box with regular grid consisting of $128 \times 128 \times 128$ grid cells with the grid spacing

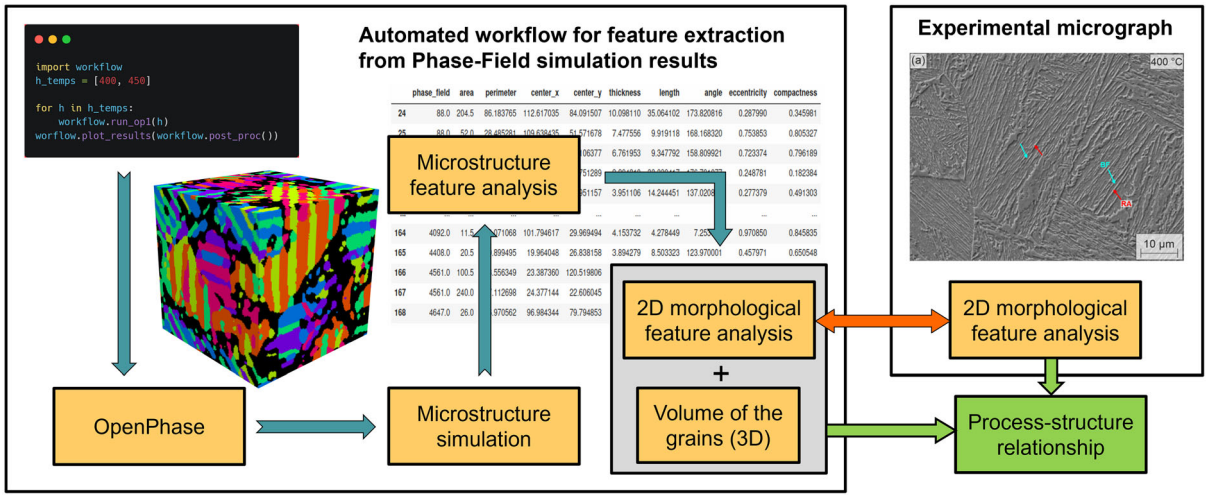


Figure 1. Automated workflow implementation to investigate the process–structure relationship for bainitic microstructure using phase-field simulation results.

© 2024 The Author(s). Advanced Engineering Materials published by Wiley-VCH GmbH

15272648, 0, Downloaded from https://onlinelibrary.wiley.com/doi/10.1002/adem.202400905 by Rwth Aachen Hochschulbibliothek, Wiley Online Library on [01/10/2024]. See the Terms and Conditions (https://onlinelibrary.wiley.com/terms-and-conditions) on Wiley Online Library for rules of use; OA articles are governed by the applicable Creative Commons License

15272648, 0, Downloaded from https://onlinelibrary.wiley.com/doi/10.1002/adem.202400905 by Rwth Aachen Hochschulbibliothek, Wiley Online Library on [01/10/2024]. See the Terms and Conditions (https://onlinelibrary.wiley.com/terms-and-conditions) on Wiley Online Library for rules of use; OA articles are governed by the applicable Creative Commons License

Table 1. List of extracted 2D morphological features.

Parameter	Description
Area	The area of the bainitic ferrite grain.
Perimeter	The perimeter of the bainitic ferrite grain.
Length	The length of the bainitic ferrite grain.
Thickness	The thickness of the bainitic ferrite grain.
Direction	Angle of the fitted ellipse around the grain.
Aspect ratio	Ratio of thickness of the bainitic ferrite grain to the length of the bainitic ferrite grain. It is one of the shape factors.
Compactness	Compactness ranges between 0 and 1. Perfect circle have a compactness of 1 and 0 indicates the lack of compactness. It is one of the shape factors.
Equivalent radius	Radius of the circle with an equal aggregate sectional area.

of 0.05 μm and periodic boundary conditions. The simulations begin at a high temperature of 627 °C, where austenite is a stable phase. Upon cooling, BF nucleates and grows from the austenite subject to driving forces depending on mechanical, chemical, and thermal conditions. The PF simulations are performed using the approach presented in ref. [20]. Within this approach, the temperature evolution in the simulations follows Newton's law of cooling, which gives realistic thermal behavior depending on the temperature difference between the sample and the cooling bath

$$\dot{T}(t) = -\beta(T(t) - T_s) + \frac{Q\dot{\phi}}{\rho C_p} \tag{1}$$

where $T(t)$ is the temperature within the sample which is considered uniform across the sample, T_s represents the temperature of the cooling bath, Q is the latent heat of transformation, ρ is the mass density, and $\dot{\phi}$ is the average rate of phase change throughout the volume of the sample. The heat extraction coefficient β, which quantifies the heat removal from the sample, is given by

$$\beta = \frac{A\alpha}{V\rho c_p} \tag{2}$$

and accounts for the type of cooling medium used, e.g., air, oil, or water. In the current study, the value for the heat extraction coefficient $\beta = 0.25\,s^{-1}$ (approximate cooling rate at the beginning of the bainite formation is $(100\,K\,s^{-1})$ used for two different isothermal holding temperatures $T_{iso} = 400$ and 450 °C.

It is known that the rapid quenching rates and lower holding temperatures can lead to the formation of lower bainite, which results in a structure closely resembling tempered martensite. In contrast to the martensite formation where no carbon partitioning is observed during the transformation and which only occurs during the subsequent tempering, during the bainite formation, the carbon partitioning and diffusion occur alongside the deformation induced transformation. Conversely, low quenching rates and higher holding temperatures can lead to the formation of upper bainite, where deformation and carbon redistribution occur concurrently.

In the current study, we limit our consideration to the formation of lower bainite. To do so, 24 different Kurdjumov–Sachs variants of BF are nucleated and grown from a single austenite grain. In this study, we do not consider cementite precipitation due to the lack of simulation resolution required by the size of the fine cementite precipitates size. The resulting microstructures considering two different values of isothermal holding temperatures (T_{iso}) are displayed in **Figure 2**a,b. Variations in the isothermal holding temperatures alter the transformation kinetics, thereby affecting the morphology of the bainitic microstructure which will be analyzed in the following sections. Figure 2c,d illustrates the carbon distribution within the sample after a simulation duration of 75 s, with isothermal holding temperatures of $T_{iso} = 400$ °C and $T_{iso} = 450$ °C, respectively. Significantly lower-carbon partitioning is observed for the isothermal holding temperature of 400 °C compared to 450 °C. And in-depth carbon composition analysis is beyond the scope of this article and will be published elsewhere.

2.3. 2D Microstructural Investigation from PF Simulation Results

To analyze the 2D morphological features of the 3D microstructures obtained from the PF simulations, a slicing operation is performed, as illustrated in **Figure 3**. The slices are taken along the (0,0,1) direction.

Traditionally, morphological features such as the area and perimeter of grains have been extracted from experimental microstructures. However, these features alone may not suffice to fully characterize the morphology, especially in the case of non-equiaxed grains where shape factors, like the aspect ratio, play a crucial role. For instance, microstructures with similar grain areas but different grain shapes can exhibit significantly different morphologies. To address this issue, additional morphological features, including shape factors, are extracted to analyze complex morphological characteristics.

Technically, 2D morphological features are obtained for each grain by masking out all other grains. The OpenCV library[22] is utilized to extract some of these morphological features. A comprehensive list of the extracted 2D morphological features is provided in Table 1.

An example of extracted morphological features can be seen in **Figure 4**. The mentioned set of features is extracted as they are commonly analyzed for experimental microstructures.[4]

2.4. 3D Microstructural Features

Most experimental studies on microstructures have traditionally been conducted in 2D, with morphological features extracted from 2D micrographs, as discussed in Section 2.3. However, the extrapolation of 2D morphological features to 3D often results in significant information loss, failing to accurately represent the true 3D characteristics of the material.[8] Key properties such as the volume of the grain and its aspect ratio are inherently 3D and cannot be fully captured through 2D analysis alone. Estimating the aspect ratio from 2D observations is particularly prone to error, given the absence of information on the third dimension.

© 2024 The Author(s). Advanced Engineering Materials published by Wiley-VCH GmbH

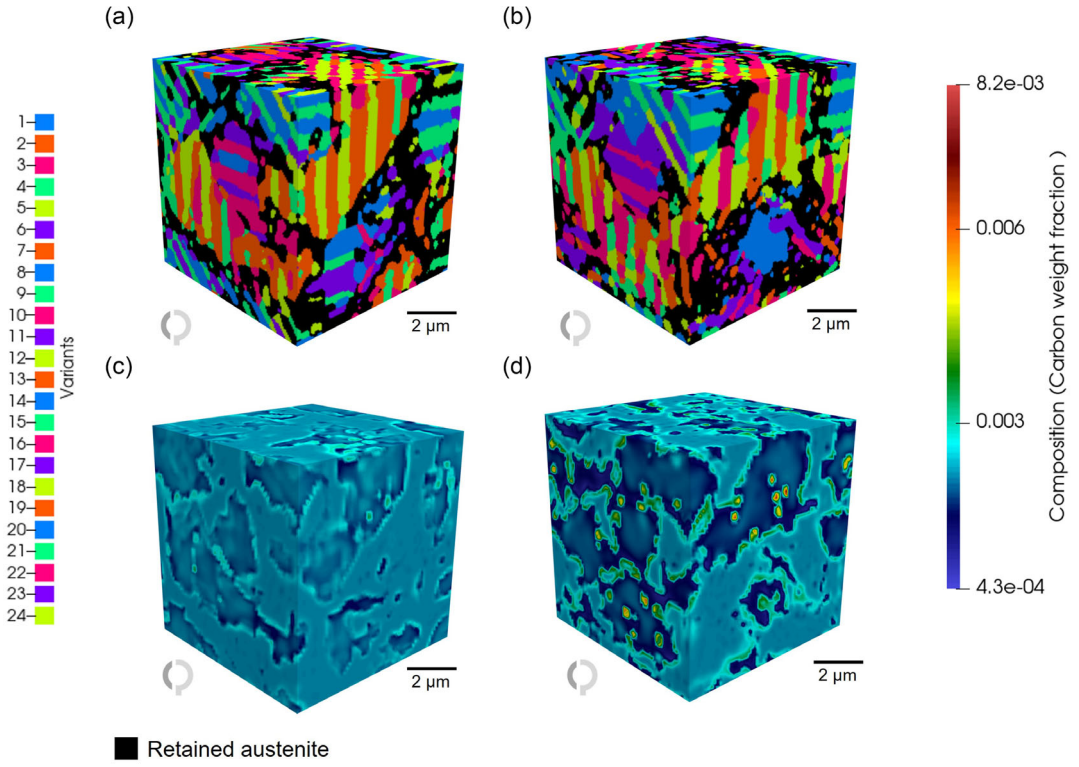


Figure 2. Bainitic microstructures simulated for two different isothermal holding temperatures: a) $T_{iso} = 400\,°C$ and b) $T_{iso} = 450\,°C$; c,d) corresponding carbon concentrations.

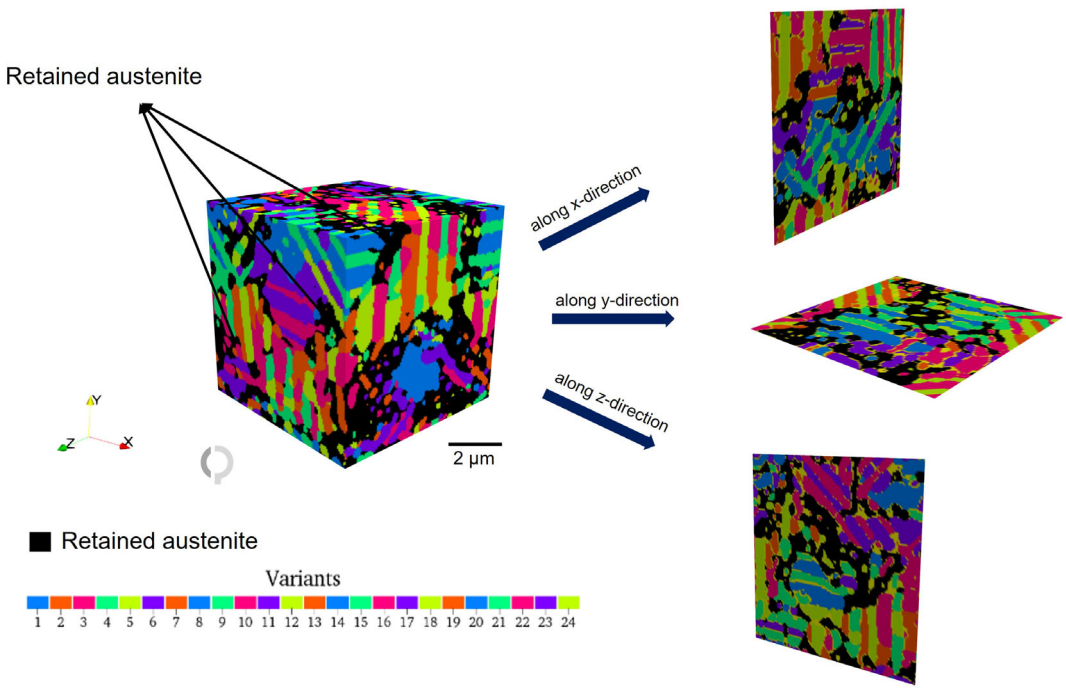


Figure 3. Automated 2D slicing as a solution to generate large datasets for effective application of ML methods.

© 2024 The Author(s). Advanced Engineering Materials published by Wiley-VCH GmbH

15272648, 0, Downloaded from https://onlinelibrary.wiley.com/doi/10.1002/adem.202400905 by Rwth Aachen Hochschulbibliothek, Wiley Online Library on [01/10/2024]. See the Terms and Conditions (https://onlinelibrary.wiley.com/terms-and-conditions) on Wiley Online Library for rules of use; OA articles are governed by the applicable Creative Commons License

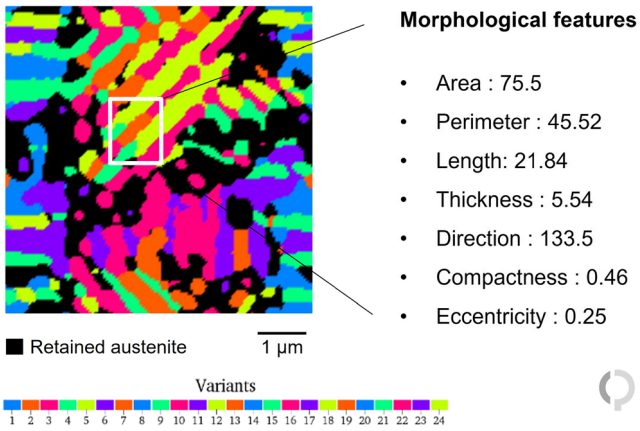


Figure 4. Extracted 2D morphological features for a grain in the white box.

The adoption of 3D morphological analysis enables a more precise differentiation between various bainite morphologies, such as lath-like bainite, which is prevalent within bainitic structures. Moreover, utilizing 3D data allows accurate identification of neighboring grains, a critical aspect to understand microstructural interactions.[23]

3. Results and Discussion

Two different carbide-free bainitic microstructures were achieved via isothermal holding for 45 min at 400 and 450 °C for Si-alloyed bainitic steel with a chemical composition shown in **Table 2**.[3] More details regarding alloy production and processes can be found in ref. [3]. Scanning electron microscope (SEM) images of two different isothermal heat treatments (quenching to a) 400 °C and b) 450 °C with 45 min of isothermal holding) are shown in **Figure 5**. SEM investigations were carried out using a field-emission gun Zeiss Sigma SEM (Carl Zeiss Microscopy GmbH, Germany). The images were acquired using a secondary electron detector with a 30 μm aperture, an accelerating voltage of 15 kV, and a working distance of 9 mm. Both the SEM microstructures exhibited platelike BF and RA films between the BF plates. An example of the areas that consisted of these morphologies is highlighted with orange-dashed lines in the microstructures. From the SEM images, it can be observed that the number of similar regions was increased in low-temperature bainite. In addition to this, it becomes clear that with decreasing the isothermal transformation temperature, a finer microstructure was obtained. Compared to the isothermal holding temperature at 450 °C, the average thickness of BF plates and RA films decreased at 400 °C. In the prior study of Gulbay et al.[3] a statistical analysis was conducted to reveal the differences in the average thickness of BF plates and RA films of these two microstructure states. In this study, the number of analyzed BF plates and RA films was extended to achieve more accurate results. For the measurements, only the platelike BF and filmlike RA morphologies were used as highlighted in the orange regions in Figure 5. Other morphologies were not included in the measurements for comparability reasons. ImageJ software was used for the thickness measurements and more than 400 measurements were accomplished using multiple SEM images for each phase of each alloy state. With decreasing isothermal holding temperature, the average thickness of BF plates decreased from 0.26 to 0.15 μm, while the width of RA films decreased from 0.25 to 0.15 μm. The summary of the statistical analysis for the thickness measurements can be found in **Table 3**.

Table 2. Chemical compositions of the material used for the experimental study. Optical emission spectroscopy (OES) was used for determining chemical composition and combustion analysis was used to estimate carbon.

Elements	C	Si	Mn	P	S	Cr	Mo	Al	Cu
wt%	0.19	1.48	2.38	0.003	0.003	0.04	0.01	0.003	0.02

Table 3. Measured average thickness of BF plates and RA films.

Heat-treatment state	Bainitic ferrite [μm]	Retained austenite [μm]
400 °C	0.15 ± 0.05	0.15 ± 0.05
450 °C	0.26 ± 0.08	0.25 ± 0.09

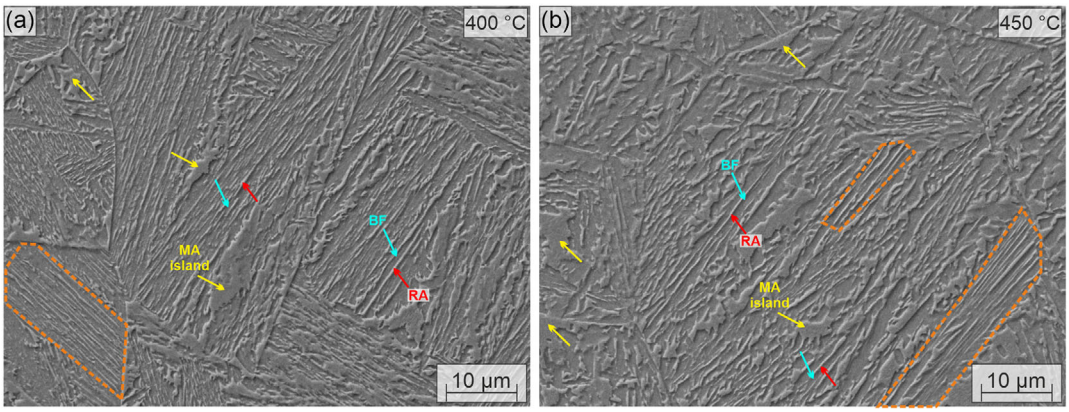


Figure 5. SEM images of microstructures isothermal obtained at a) 400 °C and b) 450 °C.

© 2024 The Author(s). Advanced Engineering Materials published by Wiley-VCH GmbH

15272648, 0, Downloaded from https://onlinelibrary.wiley.com/doi/10.1002/adem.202400905 by Rwth Aachen Hochschulbibliothek, Wiley Online Library on [01/10/2024]. See the Terms and Conditions (https://onlinelibrary.wiley.com/terms-and-conditions) on Wiley Online Library for rules of use; OA articles are governed by the applicable Creative Commons License

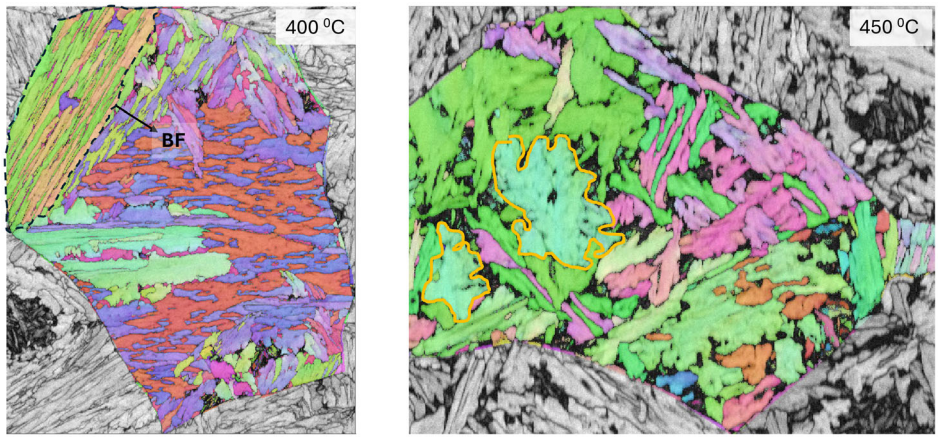


Figure 6. Inverse pole figure maps of single prior austenite grain (PAG) from holding temperatures 400 and 450 °C, respectively.

3.1. 2D Microstructural Investigations from Experimental Observations

The inverse pole figure (IPF) maps are obtained for a single prior austenite grain (PAG) for both isothermal states which are shown in **Figure 6**. The EBSD measurements were accomplished using a NordlysNano (Oxford Instruments, Great Britain) detector. For the EBSD measurements, aperture size of 75 µm, an accelerating voltage of 20 kV, a working distance of 17 mm, and a step size of 50 nm are used. EBSD post-processing is done using AZtecCrystal Software from Oxford Instruments. A single PAG is selected for comparison with simulation results. IPF map of the sample with an isothermal holding temperature of 400 °C shows thin lath-like morphologies of BF, highlighted in the black-dashed region. In contrast, the sample from the isothermal holding temperature of 450 °C shows coarser morphology of BF highlighted in the orange color. Most of the microstructure from 450 °C exhibit coarser morphology unlike in 400 °C and morphological measurements support this observation. Results reveal the similarities between experiments and simulation as they exhibit morphologies and are discussed in the following sections.

In carbide-free bainitic steels, it is well-known that excessive carbon is enriched in surrounding austenite when a BF plate is formed during the bainitic transformation.[24,25] Therefore,

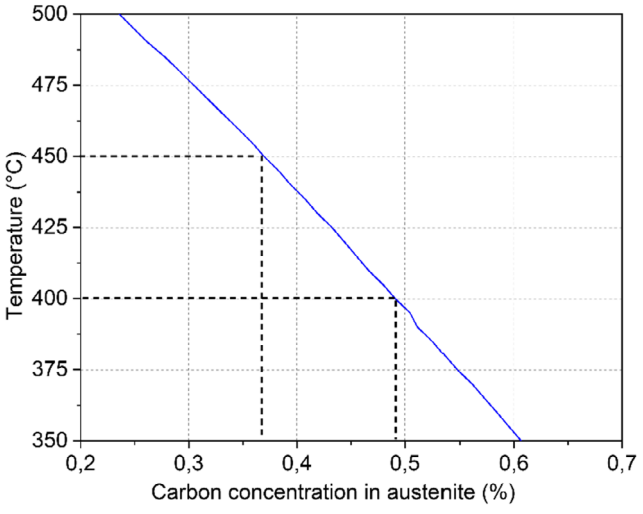


Figure 7. The T_0 curve of the studied alloy between 350 and 500 °C. 400 J mol^{-1} was included in the calculations as the strain energy of bainitic ferrite.

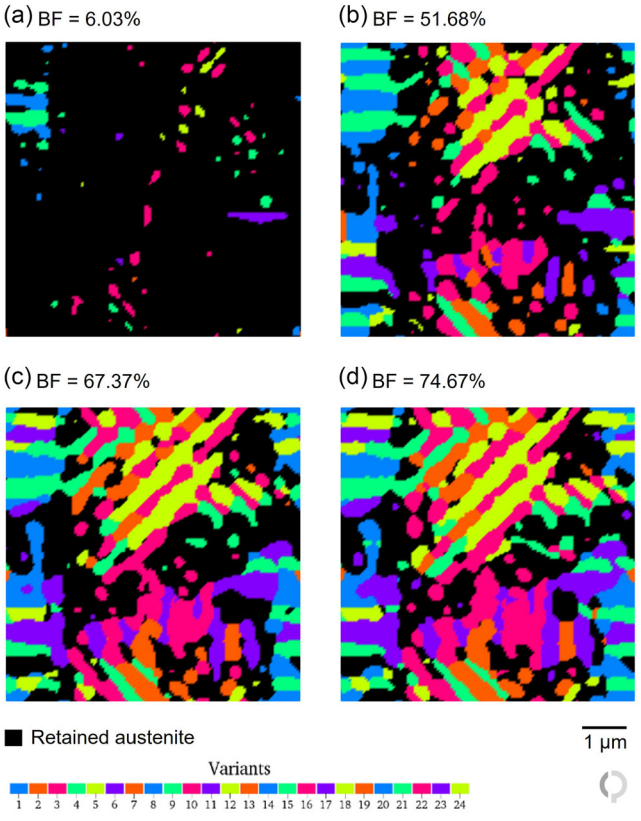


Figure 8. Evolution of bainitic ferrite (BF) microstructures for isothermal holding temperature T_{iso} = 400 °C: a) BF: 6.03%, b) BF: 51.68%, c) BF: 67.37%, and d) BF: 74.67%.

© 2024 The Author(s). Advanced Engineering Materials published by Wiley-VCH GmbH

15272648, 0, Downloaded from https://onlinelibrary.wiley.com/doi/10.1002/adem.202400905 by Rwth Aachen Hochschulbibliothek, Wiley Online Library on [01/10/2024]. See the Terms and Conditions (https://onlinelibrary.wiley.com/terms-and-conditions) on Wiley Online Library for rules of use; OA articles are governed by the applicable Creative Commons License

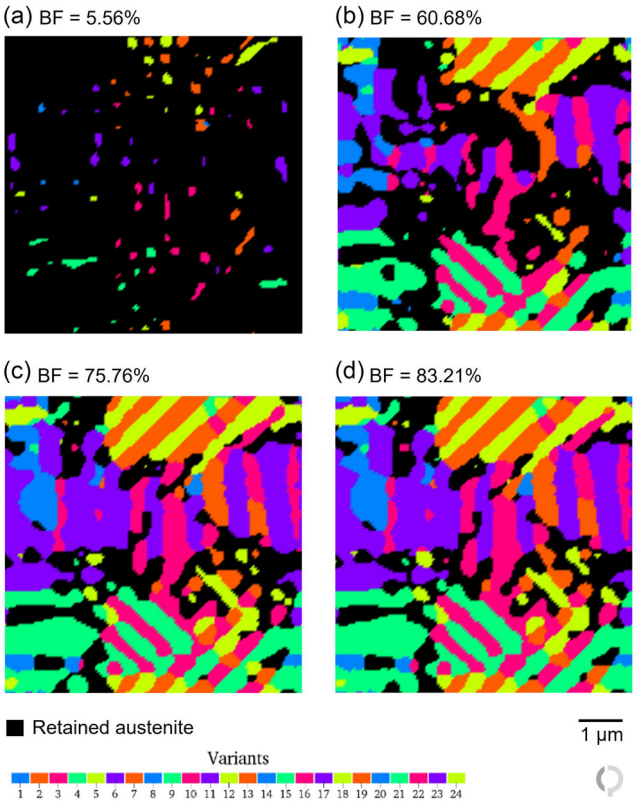


Figure 9. Evolution of bainitic ferrite (BF) microstructures for isothermal holding temperature $T_{iso} = 450\,°C$: a) BF: 5.56%, b) BF: 60.68%, c) BF: 75.76%, and d) BF: 83.21%.

carbon-enriched zones form adjacent to BF plates due to carbon partitioning and the carbon concentration in these zones decreases with an increasing distance from BF plates.[26] According to the incomplete-reaction phenomena (T0 concept), the spontaneous transformation of austenite to BF ceases when the carbon concentration in austenite reaches a threshold value. This means that a new BF plate can only form again when the carbon concentration is below a threshold value in austenite.[27] As displayed in **Figure 7**, the T_0 curve (temperature versus carbon concentration in austenite) is determined between 350 and 500 °C for this chemical composition via the thermodynamical calculations using Bhadeshia's model.[28] As highlighted in Figure 6, the carbon threshold that austenite can store increases with decreasing temperature. In other words, at 400 °C, the next BF plate starts forming at a higher carbon concentration (smaller distance) at the austenite interface compared to 450 °C, which results in finer RA films and finer microstructure. In addition to that, the mechanical strength of RA plays an important role in the thickness of the BF plates.[29] The yield strength of RA increases with decreasing transformation temperature. This enhances the resistance against growth of BF plate, which is inherited as finer BF plates in the microstructure.

Additionally, both microstructures exhibited MA islands mostly located at the PAG boundaries (PAGB), as highlighted in Figure 5. It is well accepted that there are two main types of RA in carbide-free bainitic microstructures. The first one is the nanoscale filmlike morphology, which forms between BF plates and exhibits enhanced thermal stability. The second one is relatively larger in scale and has a blocky morphology, which mostly forms at PAGB and is thermally unstable compared to the filmlike type.[30] Due to the low thermal stability of blocky RA, they are prone to transform to martensite during subsequent cooling after isothermal holding, hence the formation of MA islands.[3]

3.2. Evolution of Microstructure During Transformation in PF Simulations

Microstructure evolution of BF at two isothermal holding temperatures is presented in **Figure 8** and **9**. Unlike in experiments, we can easily track the microstructure evolution throughout the entire transformation. For the bainitic transformation with

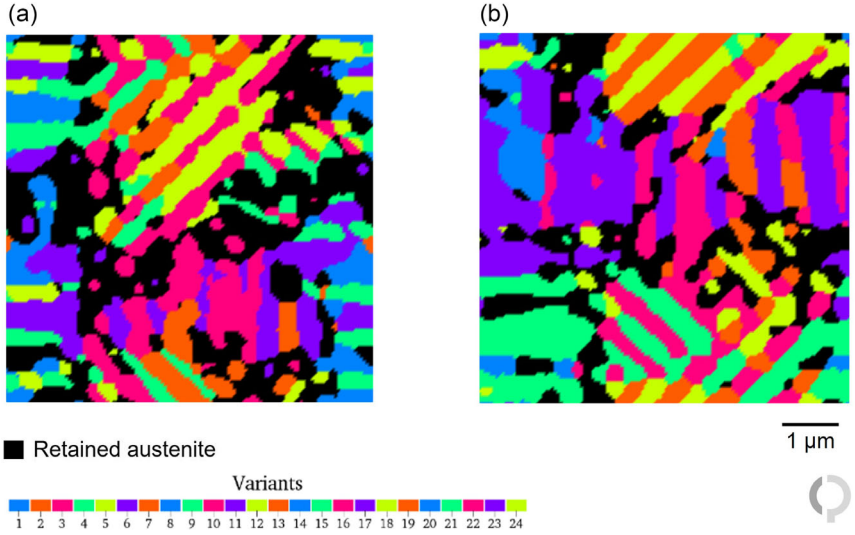


Figure 10. The 2D slice of interest for two isothermal holding temperatures: a) $T_{iso} = 400\,°C$ and b) $T_{iso} = 450\,°C$.

© 2024 The Author(s). Advanced Engineering Materials published by Wiley-VCH GmbH

15272648, 0, Downloaded from https://onlinelibrary.wiley.com/doi/10.1002/adem.202400905 by Rwth Aachen Hochschulbibliothek, Wiley Online Library on [01/10/2024]. See the Terms and Conditions (https://onlinelibrary.wiley.com/terms-and-conditions) on Wiley Online Library for rules of use; OA articles are governed by the applicable Creative Commons License

Table 4. Average values of 2D morphological features for two isothermal holding temperatures.

Parameter	$T_{iso} = 400\,°C$	$T_{iso} = 450\,°C$
Area [px]	62.11	89.84
Perimeter [px]	37.01	43.26
Length [px]	15.28	19.95
Thickness [px]	6.82	7.64
Aspect ratio	0.52	0.53
Compactness	0.58	0.58

$T_{iso} = 400\,°C$, austenite begins to break down into bainite, revealing small grains and small traces of lath-like structures of BF during the initial stages. As the bainitic transformation progresses, it becomes evident that different morphologies like lath structures and irregular polygonal structures are observed throughout the later stages.

Conversely, during the bainitic transformation with $T_{iso} = 450\,°C$, the breakdown of austenite initially favors the formation of smaller structures and irregular structures over lath-like structures. As the bainitic transformation continues, the development of irregular polygonal structures and lath-like structures is more pronounced compared to small grain-like structures. Further analysis of the microstructure morphology is presented in Section 3.3.

3.3. 2D Microstructural Investigation from PF Simulation Results

3.3.1. Morphological Feature Analysis

In the current study, BF microstructures resulting from two isothermal holding temperatures are examined as discussed in previous sections. To investigate the 2D morphology of these microstructures, a slice of interest (SOI) has been extracted from each of the two bainitic samples in the (0,0,1) direction, as illustrated in **Figure 10**. We have detailed information on the phase and the variants of BF for every pixel within the SOI from the PF simulation results using OpenPhase.[18] This information provides an additional advantage for more precise analysis of the microstructures. The morphological features of the microstructure, outlined in Table 1, are quantified for each grain. The total counts of grains in the slices are 123 and 143, respectively. The proportions of RA in the SOIs are 25.33% and 16.76%, respectively. Grains smaller than ten pixels have been excluded from consideration to minimize the effect of the numerical discretization limit of PF simulations. Average values of certain morphological features across all grains are summarized in **Table 4**. These measurements are provided in pixels, with a conversion factor of 1 µm equaling 20 pixels (px).

According to the data presented in Table 4, it is evident that the average grain size, measured in terms of area, is smaller for grains resulting from lower holding temperature compared to higher holding temperature. These findings align with previous

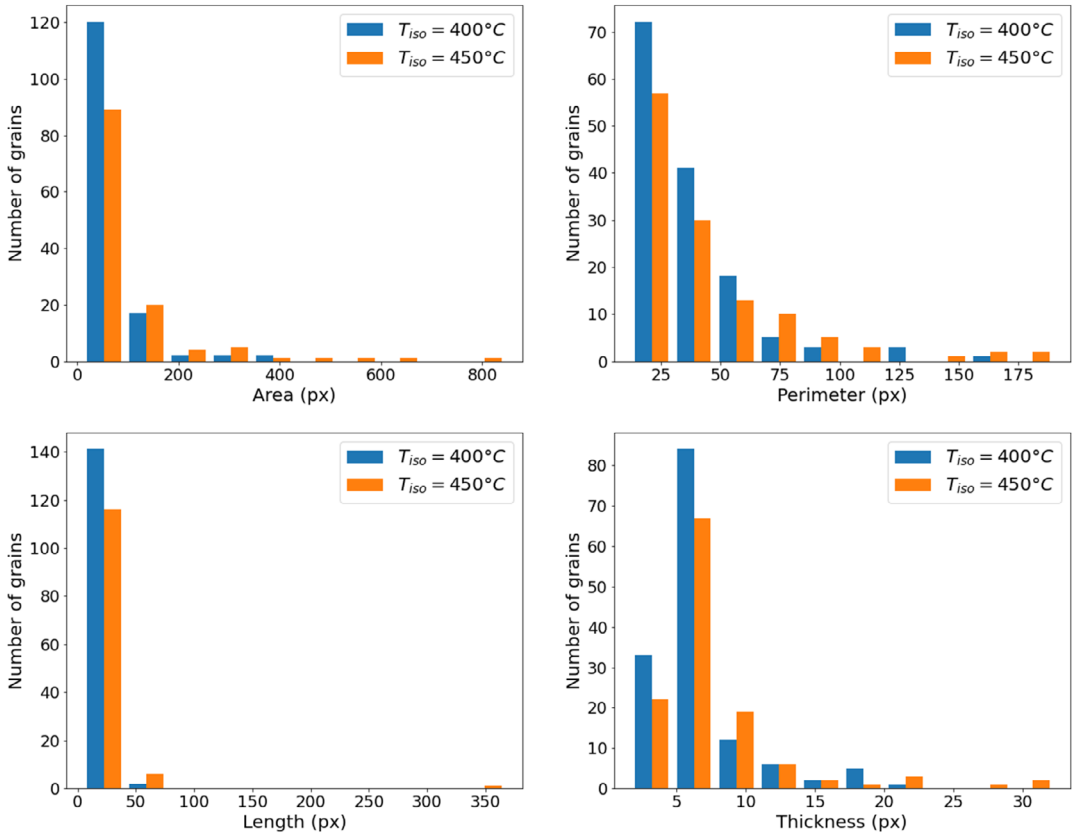


Figure 11. Distribution of different morphological parameters of all grains.

© 2024 The Author(s). Advanced Engineering Materials published by Wiley-VCH GmbH

15272648, 0, Downloaded from https://onlinelibrary.wiley.com/doi/10.1002/adem.202400905 by Rwth Aachen Hochschulbibliothek, Wiley Online Library on [01/10/2024]. See the Terms and Conditions (https://onlinelibrary.wiley.com/terms-and-conditions) on Wiley Online Library for rules of use; OA articles are governed by the applicable Creative Commons License

experimental studies in ref. [3]. Also, coarser BF is observed at high holding temperature from simulations and experiments which can be seen in Figure 6 and 10.

This observation is particularly significant as it provides insights into the influence of isothermal holding temperatures on microstructural characteristics. However, examining the average grain size alone may not fully capture the distribution of grain sizes within the microstructure. For a more comprehensive understanding, the distribution of grain sizes across the sample can be visualized, as depicted in **Figure 11**. This distribution allows for a more detailed analysis of the variations in grain sizes and their implications on the overall microstructure.

In the present work, we attribute the microstructures to lath bainite. The designations of these morphologies are taken from refs. [31,32].

The analysis of grain area distribution shows a sharp decrease in grain size at both holding temperatures. Specifically, at lower holding temperature, no grains exceed 400 pixels in area, while at higher holding temperature, only a few grains are larger than 400 pixels. A similar pattern is observed in the perimeter distribution, though it shows a smoother decreasing trend compared to the area distribution.

Regarding grain length distribution, most grains are under 50 pixels in length at both isothermal holding temperatures, with only a few grains around 50 pixels. In contrast, the thickness distribution does not exhibit a clear trend for either temperature setting. However, the data suggests that grains are thinner at the lower holding temperature compared to the higher one, indicating finer grains at the lower holding temperature—a finding that aligns with experimental observations.

The average thickness of the grains is measured at 0.341 and 0.382 μm for the low and high holding temperatures, respectively. However, the experimental data shows an average grain thicknesses of 0.15 ± 0.05 and 0.26 ± 0.08 μm for holding temperatures of 400 and 450 °C, respectively. This points to a discrepancy in the simulated results for the lower holding temperature which could be due to the simulation resolution limit, although the high holding temperature results are closely aligned with the experimental findings.

3.4. 3D Microstructure Analysis

Utilizing 3D microstructure analysis, one can achieve accurate quantification of the volume fractions of various phases, as well as ascertain the morphology of these phases. As illustrated in **Figure 12**, the grains display both lath-like and platelike structures. In this study, the volume of each grain is calculated, which is derived from PF simulations. Given the irregular shapes of the grains, this opens up opportunities for exploring different shape factors to better estimate the grain's morphology. Although we attempted to use an ellipsoidal fit to characterize these shapes, the method proved ineffective due to the grain's irregular geometries.

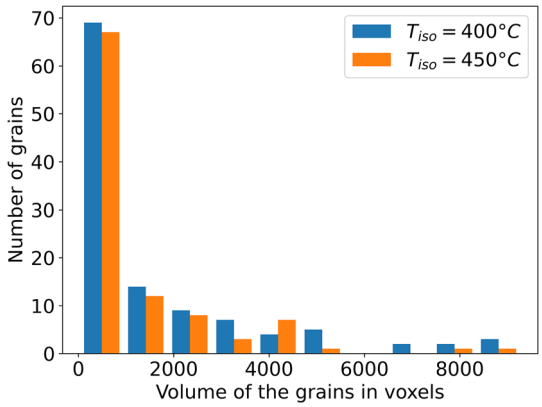


Figure 13. Distribution of volume of the grains in voxels for two isothermal holding temperatures.

The grain size distribution, in terms of the volume of the grains, is depicted in **Figure 13**. This distribution clearly shows that a lower holding temperature results in a higher number of very small grains (less than 2000 voxels). As the grain size surpasses 5000 voxels, the frequency of grains decreases significantly at higher holding temperature compared to low holding temperature, indicating a reduced number of grains in the specimens. This trend demonstrates a general decrease in grain size with lower holding temperature.

4. Conclusion

In this study, we successfully employed an automated workflow implementation to simulate low-carbon bainitic steels under different isothermal holding temperatures using the PF software library OpenPhase. We examined the effect of isothermal holding temperature on the microstructure morphology and

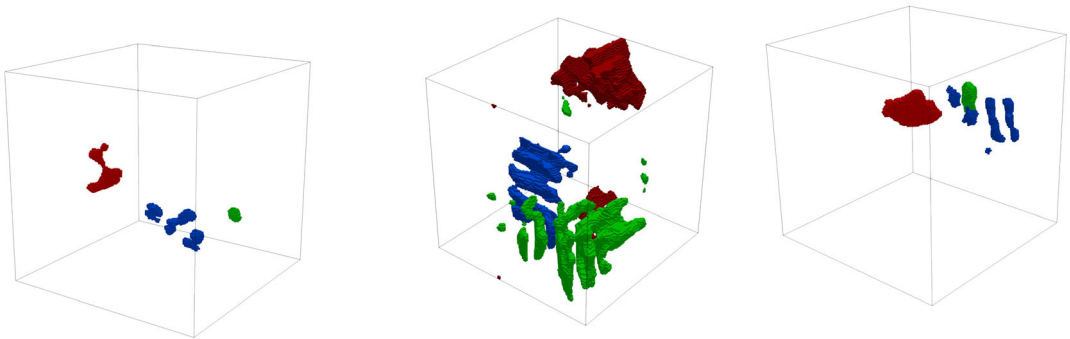


Figure 12. Different bainitic microstructures showing platelike morphology and complex morphology in 3D space.

© 2024 The Author(s). Advanced Engineering Materials published by Wiley-VCH GmbH

15272648, 0, Downloaded from https://onlinelibrary.wiley.com/doi/10.1002/adem.202400905 by Rwth Aachen Hochschulbibliothek, Wiley Online Library on [01/10/2024]. See the Terms and Conditions (https://onlinelibrary.wiley.com/terms-and-conditions) on Wiley Online Library for rules of use; OA articles are governed by the applicable Creative Commons License

conducted comparisons with experimental findings. Analysis of morphological features indicates that grains decrease in size at lower holding temperature compared to high holding temperature. This is also supported by the 3D grain size distribution. The key findings of this research can be summarized as follows. 1) Microstructural features like thickness of the BF are calculated from experiments and simulations for two different heat-treatment conditions. Average grain thickness at high temperatures from simulations and experiments is qualitatively aligned, whereas at low temperature, measurements from experiments and simulations show discrepancies. 2) The grain length distribution from the PF simulation results illustrates that microstructures with a low holding temperature exhibit finer grains, implying smaller grain sizes. Simultaneously, the thickness distribution plot demonstrates that grains are becoming thinner overall. 3) The grain area and perimeter distributions show a sharp decrease at low and high isothermal holding temperatures. And no grains have exceed 400 pixels in area at lower temperatures, with only a few larger grains at higher temperatures. 4) Most of the grains are under 50 pixels in length at both temperatures, with few reaching around 50 pixels. Grain thickness does not show a clear trend, but grains appear thinner at lower temperatures, indicating finer grains. 5) Further work is required to analyze 3D morphologies as they exhibit complex structures. And new shape factors should be employed to evaluate these structures further.

Acknowledgements

The authors acknowledge funding by the German Federal Ministry of Education and Research (BMBF)—project 13XP5118A (iBain).

Open Access funding enabled and organized by Projekt DEAL.

Conflict of Interest

The authors declare no conflict of interest.

Author Contributions

Dhanunjaya Nerella: Data curation: (lead); Formal analysis: (lead); Methodology: (equal); Software: (equal); Writing—original draft: (lead); **Muhammad Adil Ali**: Methodology: (supporting); Software: (supporting); Writing—original draft: (supporting); **Hesham Salama**: Formal analysis: (supporting); Methodology: (supporting); Software: (supporting); Writing—original draft: (supporting); **Oguz Gülbay**: Data curation: (equal); Formal analysis: (equal); Methodology: (supporting); Software: (supporting); Writing—original draft: (supporting); **Marc Ackermann**: Data curation: (equal); Formal analysis: (equal); Supervision: (equal); Writing—review and editing: (supporting); **Oleg Shchyglo**: Methodology: (equal); Project administration: (lead); Software: (supporting); Supervision: (equal); Writing—review and editing: (lead); **Ulrich Krupp**: Funding acquisition: (equal); Project administration: (equal); Supervision: (equal); Writing—review and editing: (supporting). **Ingo Steinbach**: Conceptualization: (lead); Funding acquisition: (lead); Project administration: (lead); Resources: (lead); Supervision: (equal); Writing—review and editing: (equal).

Data Availability Statement

The data that support the findings of this study are available from the corresponding author upon reasonable request.

Keywords

bainite, microstructure, morphological features, workflow

Received: April 15, 2024
Revised: August 26, 2024
Published online:

[1] H. K. D. H. Bhadeshia, J. Christian, *Metall. Trans. A* **1990**, *21*, 767.
[2] L. Fielding, *Mater. Sci. Technol.* **2013**, *29*, 383.
[3] O. Gulbay, M. Ackermann, A. Gramlich, A. R. Durmaz, I. Steinbach, U. Krupp, *Steel Res. Int.* **2023**, *94*, 2300238.
[4] D. Iren, M. Ackermann, J. Gorfer, G. Pujar, S. Wesselmecking, U. Krupp, S. Bromuri, *Sci. Data* **2021**, *8*, 140.
[5] M. Ackermann, D. Iren, S. Wesselmecking, D. Shetty, U. Krupp, *Mater. Charact.* **2022**, *191*, 112091.
[6] X. Long, J. Kang, B. Lv, F. Zhang, *Mater. Des.* **2014**, *64*, 237.
[7] W. L. Costin, O. Lavigne, A. Kotousov, *Mater. Sci. Eng. A* **2016**, *663*, 193.
[8] Y. Jiang, M. A. Ali, I. Roslyakova, D. Bürger, G. Eggeler, I. Steinbach, *Modell. Simul. Mater. Sci. Eng.* **2023**, *31*, 035005.
[9] P. Steinmetz, Y. C. Yabansu, J. Hötzer, M. Jainta, B. Nestler, S. R. Kalidindi, *Acta Mater.* **2016**, *103*, 192.
[10] Y. C. Yabansu, P. Steinmetz, J. Hötzer, S. R. Kalidindi, B. Nestler, *Acta Mater.* **2017**, *124*, 182.
[11] H. S. Stein, J. M. Gregoire, *Chem. Sci.* **2019**, *10*, 9640.
[12] K. Mathew, J. H. Montoya, A. Faghaninia, S. Dwarakanath, M. Aykol, H. Tang, I.-h. Chu, T. Smidt, B. Bocklund, M. Horton, J. Dagdelen, B. Wood, Z.-K. Liu, J. Neaton, S. P. Ong, K. Persson, A. Jain, *Comput. Mater. Sci.* **2017**, *139*, 140.
[13] P. Nikolaev, D. Hooper, N. Perea-Lopez, M. Terrones, B. Maruyama, *ACS Nano* **2014**, *8*, 10214.
[14] T. Dimitrov, C. Kreisbeck, J. S. Becker, A. Aspuru-Guzik, S. K. Saikin, *ACS Appl. Mater. Interfaces* **2019**, *11*, 24825.
[15] C. R. Rêgo, J. Schaarschmidt, T. Schlöder, M. Penaloza-Amion, S. Bag, T. Neumann, T. Strunk, W. Wenzel, *Front. Mater.* **2022**, *9*, 877597.
[16] J. Janssen, S. Surendralal, Y. Lysogorskiy, M. Todorova, T. Hickel, R. Drautz, J. Neugebauer, *Comput. Mater. Sci.* **2019**, *163*, 24.
[17] G. Van Rossum, F. L. Drake, in *Python 3 Reference Manual*, CreateSpace, Scotts Valley, CA **2009**.
[18] OpenPhase, OpenPhase Software Library for Phase-Field Simulations, https://openphase.rub.de, (accessed: January **2024**).
[19] M. Tegeler, O. Shchyglo, R. D. Kamachali, A. Monas, I. Steinbach, G. Sutmann, *Comput. Phys. Commun.* **2017**, *215*, 173.
[20] I. Steinbach, M. Uddagiri, H. Salama, M. A. Ali, O. Shchyglo, *MRS Bull.* **2024**, *49*, 1.
[21] A. Clark, Pillow (Pil Fork) Documentation, https://buildmedia.readthedocs.org/media/pdf/pillow/latest/pillow.pdf, (accessed: January **2024**).
[22] G. Bradski, *Dr. Dobb's J.* (accessed: January **2024)**.
[23] M. Groeber, M. Uchic, D. Dimiduk, Y. Bhandari, S. Ghosh, *J. Comput.-Aided Mater. Des.* **2007**, *14*, 63.
[24] B. Sandvik, H. Nevalainen, *Met. Technol.* **1981**, *8*, 213.
[25] E. Kozeschnik, H. Bhadeshia, *Mater. Sci. Technol.* **2008**, *24*, 343.
[26] L. Chang, H. Bhadeshia, *Mater. Sci. Technol.* **1995**, *11*, 874.
[27] H. Bhadeshia, D. Edmonds, *Acta Metall.* **1980**, *28*, 1265.
[28] M. Peet, *Materials Algorithms Project Program Library*, **2007**.
[29] E. Swallow, H. Bhadeshia, *Mater. Sci. Technol.* **1996**, *12*, 121.
[30] H. Bhadeshia, D. Edmonds, *Met. Sci.* **1983**, *17*, 411.
[31] S. Zajac, V. Schwinn, K. Tacke, in *Materials Science Forum*, Vol. *500*, Trans Tech Publ., Stafa-Zurich, Switzerland **2005**, pp. 387–394.
[32] F. Caballero, H. Roelofs, S. Hasler, C. Capdevila, J. Chao, J. Cornide, C. Garcia-Mateo, *Mater. Sci. Technol.* **2012**, *28*, 95.

© 2024 The Author(s). Advanced Engineering Materials published by Wiley-VCH GmbH

15272648, 0, Downloaded from https://onlinelibrary.wiley.com/doi/10.1002/adem.202400905 by Rwth Aachen Hochschulbibliothek, Wiley Online Library on [01/10/2024]. See the Terms and Conditions (https://onlinelibrary.wiley.com/terms-and-conditions) on Wiley Online Library for rules of use; OA articles are governed by the applicable Creative Commons License